Morphology and composition of Au catalysts on Ge(111) obtained by thermal dewetting

S. Hajjar,[1] G. Garreau,[1] L. Josien,[1] J. L. Bubendorff,[1] D. Berling,[1] A. Mehdaoui,[1] C. Pirri,[1,*] T. Maroutian,[2] C. Renard,[2] D. Bouchier,[2] M. Petit,[3] A. Spiesser,[3] M. T. Dau,[3] L. Michez,[3] V. Le Thanh,[3] T. O. Mentes,[4] M. A. Nino,[4] and A. Locatelli[4]

[1]*IS2M, Université de Haute Alsace, CNRS-LRC 7228, F-68057 Mulhouse, France*

[2]*IEF, Université Paris-Sud, UMR 8622, Orsay F-91405, France and CNRS, F-91405 Orsay, France*

[3]*CINaM-CNRS, Aix-Marseille Université, Campus de Luminy, Case 913, F-13288 Marseille Cedex 9, France*

[4]*Sincrotrone Trieste, Area Science Park, Trieste I-34012, Italy*

(Received 27 May 2011; revised manuscript received 25 August 2011; published 30 September 2011)

We investigate the chemical and morphological structure of the Au nanodots on Ge(111), which serve as catalysts for the formation of epitaxial Ge nanowires. We show that dewetting of an Au film on Ge(111) gives rise to a thin Au-Ge wetting layer and Au-Ge dots. These dots are crystallized but not with a single crystallographic orientation. Thanks to the spatially resolved x-ray and transmission electron microscopy measurements, a chemical characterization of both binary Au-Ge catalysts and wetting layer is obtained at the nanoscale. We show that Ge vertical growth is achieved even without an external Ge supply.

DOI: 10.1103/PhysRevB.84.125325 PACS number(s): 81.07.−b, 61.46.−w, 81.16.−c, 68.37.Ef

I. INTRODUCTION

The growth of nanowires by the vapor-liquid-solid (VLS) or vapor-solid-solid (VSS) mechanism is a well-known and very nice bottom-up approach in the fabrication of one-dimensional objects, which can be used in a very large variety of devices.[1–5] The experimental VLS approach needs alloys that can form nanoscale catalysts, which melt at low temperatures thanks to the deep eutectic point in the bulk phase diagram. Most interesting is that these alloys are also of interest in the overall microelectronic area as solder materials and in all technological areas in which low temperature and corrosion resistance are required, such as space technology, gas sensor, and medical devices. The nanowires geometry is ideal for monolithic integration of semiconductor materials with different lattice constants due to their ability to accommodate strain in two dimensions. As to nanowires growth, if an epitaxial growth is required to perform devices, these catalysts are formed under ultrahigh vacuum on a clean and crystalline substrate. In some cases, their chemical and morphological properties have been investigated. Nevertheless, the chemical reaction at the interface between the deposited material, which serves to form the catalysts, and the semiconductor surface strongly depends on their chemical nature. There have been extensive studies on this point focusing in the formation of quasi-two-dimensional (quasi-2D) thin layers and interfaces, however, surfaces on which dots are formed present a greater challenge.

On one hand, it needs particular tools for local measurements and on the other hand, the reduced size of the catalysts and of the resulting wires introduces new phenomena. Numerous materials have been tentatively used as catalysts, each with its own influence on the nanowires growth, such as nanowires crystal orientation and growth orientation with respect to the semiconductor surface. Among these catalysts, Au droplets have been extensively used[5–41] and a particular attention is given at the nanowire-catalyst interface.[15,18–20,22,23,25–30] For other purposes, the Au-Ge(111) interface below 1 monolayer has thoroughly been investigated by photoemission, Auger electron spectroscopy, low-energy electron diffraction (LEED), and x-ray diffraction. [42–49] It is characterized by the formation of a $\sqrt{3} \times \sqrt{3} R30^\circ$ superstructure (or wetting layer) associated with the formation of Au trimers on Ge(111).[47–49] It is found to be stable at high annealing temperatures, up to the melting point of germanium.[44] In contrast, the Au/Ge(111) interface has only poorly been studied for Au deposits above 1 monolayer. It is worth noting that Au catalysts are generally created by dewetting a pure Au film of about 1 nm thick and up to now only few papers report on the characterization of the Au droplets before nanowires growth.

In this work, we investigate both chemical and morphological structure of the Au platelets on Ge(111), formed by annealing a pure Au film at a temperature below 300 °C, and of Au droplets, formed at higher annealing temperature, which serve as catalysts for the formation of epitaxial Ge nanowires. This study is performed by using scanning tunneling microscopy (STM), x-ray photoemission spectroscopy (XPS) and x-ray photodiffraction (XPD), reflection high-energy electron diffraction (RHEED), and finally by using x-ray photoemission electron microscopy (XPEEM) and transmission electron microscopy (TEM) in both image and microanalysis modes.

II. EXPERIMENT

The sample preparation, as well as the STM, RHEED, and x-ray photoelectron diffraction (XPD) measurements, were performed in UHV setup with a base pressure below 1×10^{-10} mbar. STM measurements were made in a room-temperature-operating microscope (Omicron STM-AFM microscope), in the constant-current mode. Electrochemically etched, *in situ* cleaned tungsten tips were used. The Au catalysts were grown on a clean Ge(111) substrate. The Ge(111) substrate was degassed by direct heating up to 450 °C for 10 h and flashed afterwards at 720 °C to remove the native oxide layer. After repeated flashes at 720 °C for increasing durations (up to 1 min), the substrate was cooled rapidly down to 620 °C and then more slowly (at a rate of 0.5 °C/s) down to RT. STM images taken on a clean Ge(111) substrate show terraces larger than 200 nm and a quite defect-free $c(2 \times 8)$ surface atomic structure. Au catalysts were formed by annealing Au layers evaporated on such a Ge(111) substrate

kept at room temperature. An effusion cell was used with a deposition rate of about 0.05 nm/min. The Au layer thickness was set between 0.8 and 1.2 nm. This Au amount gave us the opportunity to form Au-Ge droplets with a lateral size between 5 and 200 nm, then easily observable by STM for the smallest one, and by SEM and x-ray spectromicroscopy for the largest. The deposition rate is controlled by a water-cooled quartz crystal microbalance and the nominal Au thickness is given with a precision better than 10%. The annealing temperature is monitored with an accuracy of ± 20 °C. XPD measurements were carried out using a hemispherical analyzer operating at an angular resolution of $\pm 1^\circ$ (Omicron experimental setup). XPD scans were obtained by measuring the intensity of the Au 4*f* core-level doublet excited with an Al $K\alpha$ x-ray source (photon energy = 1486.6 eV).

The local x-ray spectromicroscopy measurements are performed with the spectroscopic photoemission and low-energy electron microscope (SPELEEM) at Elettra laboratory in Trieste (Italy) on the Nanospectroscopy beamline, which routinely works with spatial resolution of 40 nm in XPEEM mode. Details on the microscope and the beamline are reported in Refs. 50 and 51. Using synchrotron light as a photon source we were able to select the photon energy for probing both Ge 3*d* and Au 4*f* core-level emission under optimal conditions. TEM and energy dispersive x-ray spectroscopy (EDX) were performed with a JEOL 3010 microscope operating at 300 keV with a spatial resolution of about 2 nm.

III. RESULTS AND DISCUSSION

Figure 1(a) shows an image of a 0.8-nm-thick Au layer deposited at room temperature on Ge(111). The Au film is rather flat and covers quite uniformly the Ge surface. The LEED and RHEED pattern is 1×1 and shows that Au is ordered (in epitaxy) on Ge(111), in agreement with previous findings.[44,45] XPD Au $4f_{7/2}$ line intensity scans versus polar angle θ along the [11-2], [−1-12] and [10-1] directions of the Ge(111) crystal are shown in Fig. 1(b). The polar angle θ is defined with respect to the surface normal. These intensity modulations versus polar angle show intensity maxima at selected polar angles, consistent with the formation of a face-centered-cubic Au structure, with Au(111) // Ge(111), and with [11-2], [−1-12], and [10-1] directions of Au aligned with that of Ge(111), as observed in Ref. 44.

The Au layer is scattered into small islands upon a mild annealing at 300 °C, as shown in Fig. 2. This is the first stage of the dewetting process. The STM image shows numerous flat platelets with different lateral size and height. Their height varies from 2.5 to 4.5 nm for a nominal deposit of 0.8 nm and an annealing at 300 °C for 10 min. A line scan across two islands is shown in Fig. 2. As to their structure, Fig. 2 also shows a XPD Au $4f_{7/2}$ profile (i) versus polar angle θ along the [11-2] direction of the Ge(111) substrate. It is compared to that measured on the room-temperature deposited Au layer (ii). This close similarity shows that the Au platelets are still in epitaxy and single-oriented on the Ge(111) substrate. At this stage, an estimation of the Au platelet volume, with respect to the initial Au deposit, suggests that they are quite pure Au. Thus we may assume here that the bare surface does not significantly contribute to the Au 4*f* modulations versus polar angle. The relevance of this point will be discussed later.

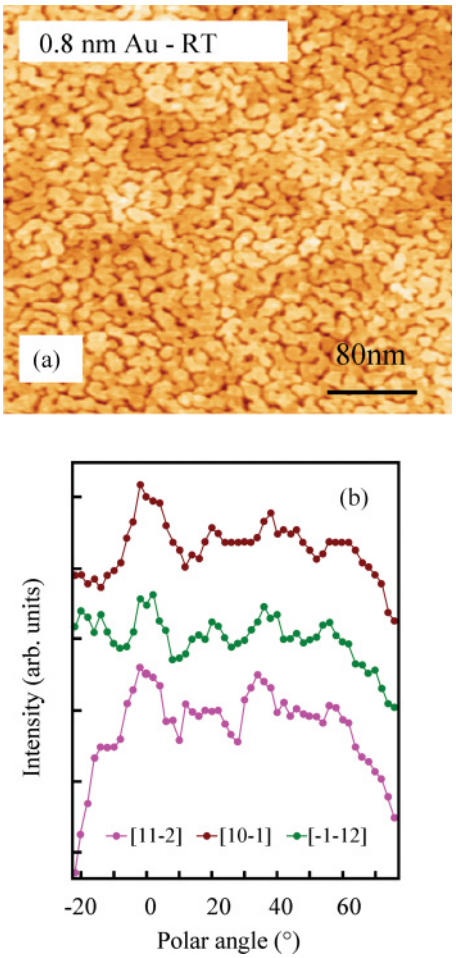

FIG. 1. (Color online) (a) STM image of 0.8-nm Au deposited onto a room-temperature (RT) clean Ge(111). (b) Au $4f_{7/2}$ XPD profiles versus polar angle θ along the [11-2], [10-1], and [−1-12] direction of the Ge(111) substrate.

Figure 3 shows a typical STM image acquired after a subsequent anneal at 325 °C for 10 min. This extra anneal does not change the overall surface morphology. Nevertheless, a close examination shows that several islands have changed their shape. A line scan across these two types of islands clearly shows flat islands and domelike islands (labeled A and B, respectively). The line scan shows that the dome island height is at least twice that of the flat island. The morphology change observed at this temperature can be attributed to the formation of Au-Ge droplets at the eutectic composition and thus Ge incorporation. From the bulk Au-Ge phase diagram, the droplet could incorporate 28 at % Ge at the eutectic temperature T_E. This would increase the domelike islands' volume of about 33% if we assume that the bulk phase diagram predictions are still correct for the small droplets and if the Ge incorporated at T_E remains within the islands at room temperature. This latter point strongly depends on the time used to decrease the sample temperature from 325 °C down to room temperature. In the present experiments, this time was rather short (less than 5 min) and we can assume that the droplet composition is quenched or partially quenched. This point will

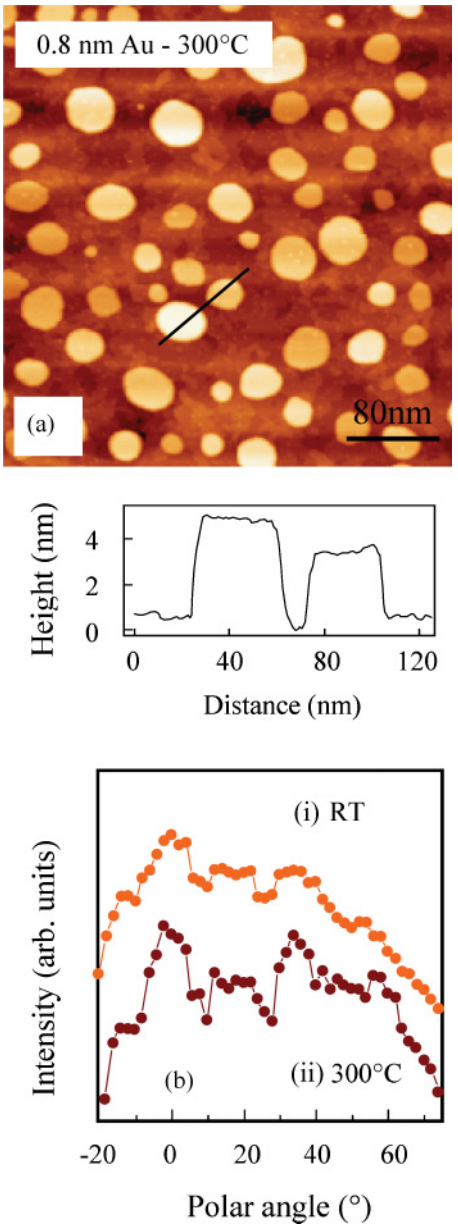

FIG. 2. (Color online) (a) STM images of 0.8-nm Au deposited onto a room-temperature (RT) clean Ge(111) annealed for 10 min at 300 °C. Also shown in this image is a line profile across islands. (b) Au $4f_{7/2}$ XPD profile versus polar angle θ along the [11-2] direction of the Ge(111) substrate measured on the Au deposit annealed at 300 °C (i) and on the as-deposited Au layer (ii).

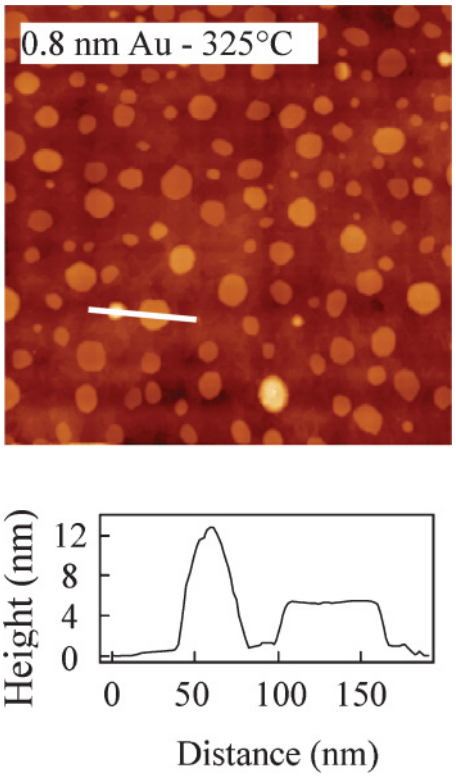

FIG. 3. (Color online) STM images of 0.8-nm Au deposited onto a room-temperature (RT) clean Ge(111) annealed for 10 min at 325 °C. Also shown in this image is a line profile, which clearly distinguishes flat and domelike islands.

be also discussed later on the basis of SEM experiments. Upon increasing the annealing temperature up to 350 °C, the surface morphology has completely changed, as evidenced in Fig. 4. This STM image is acquired after annealing the surface at 350 °C for 10 min. The platelets have completely disappeared. All islands now have a dome shape. Upon increasing the annealing time at 350 °C, the Ostwald ripening process induced a modification of the sample surface: the islands' density is reduced upon increasing annealing time, while their height and diameter increases. Figure 5 gives an STM image of the surface after 12 h annealing at 350 °C. Au droplets as large as 100 nm are now formed. These droplets are crystallized and show facets. At a first sight, all droplets do not show facets in the same crystallographic direction, as it would be expected for an Au island in epitaxy on Ge(111). A detailed view of a droplet is shown in Fig. 5. Note that the ripening process is a limiting factor in the fabrication of nanowires with low size dispersion. Despite the well defined crystallographic phases, the Au $4f_{7/2}$ intensity modulation versus θ is completely lost on the sample annealed at 350 °C. There is no more coherence between the droplets' orientation after melt. Such a profile indicates the formation of several nanocrystal orientations, as it is for a polycrystalline surface. Note that a similar Au $4f_{7/2}$ intensity modulation versus θ is measured for an annealing temperature of 400 °C.

To summarize, an overview of the evolution of the surface morphology versus annealing temperature at a given annealing time, versus annealing time at a given temperature, and versus Au layer thickness in a range generally used for nanowires growth is shown in Fig. 6. Figure 6(a) shows a set of STM images taken in the constant current mode for different Au layer thickness annealed at 350 °C (T_E). Figures 6(b)–6(d) show the mean droplet diameter, the mean droplet height, and the droplet density versus annealing duration at 350 °C for an Au deposit of 0.8 nm, respectively. The mean diameter, the mean islands' height, and the surface coverage were determined for each annealing temperature over more than 20 STM images, measured in a 2-μm × 2-μm or in a 1-μm × 1-μm (or less for the smallest droplets) -wide mode. This was also controlled on SEM images, over more than ten images for each annealing temperature with the same scanning window.

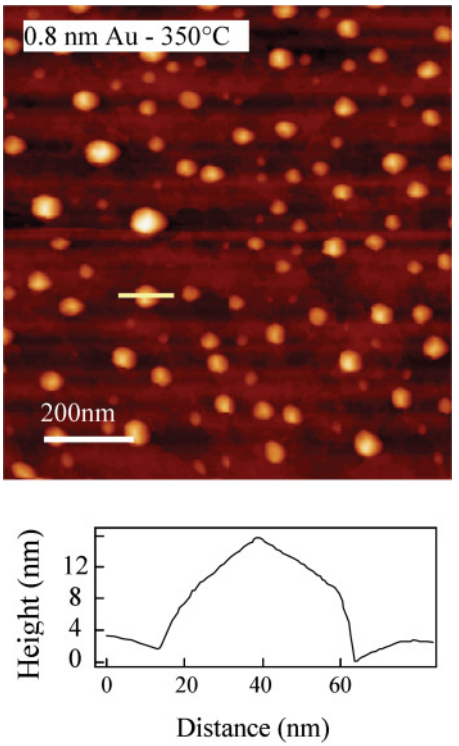

FIG. 4. (Color online) STM images of 0.8-nm Au deposited onto a room-temperature (RT) clean Ge(111) annealed for 10 min at 350 °C. Also shown in this image is a line profile across a domelike island.

It is shown that the droplet density decreases as the mean droplet diameter and height increases, versus annealing time. In particular, it was shown that the mean droplet diameter increases continuously, quite linearly, versus annealing time, even for durations as long as 12 h.

Some comment must be given about the *in situ* determination of the solid-liquid transition temperature of the droplets. We have chosen to estimate the transition temperature T_E by using the change on STM images acquired at room temperature. We have determined the temperature at which the platelets transform into dome-shaped islands (droplets) and assumed that it is T_E, indeed. This temperature is estimated for annealing time longer than 1 h. RHEED can also confirm the structural transition from crystallized platelets (2D crystals) to liquid droplets (3D liquid). RHEED measurement gives complementary and valuable information on the droplets structure. Starting from a clean Ge(111) surface characterized by a $c(2 \times 8)$ or (2×1) pattern, a (1×1) streaky RHEED pattern is observed for room-temperature Au deposition up to a thickness of 1.2 nm. This indicates that the deposited Au film is relatively flat and epitaxial, in agreement with STM and XPD results. Figure 7(a) displays a RHEED pattern taken along the [1-10] azimuth of a 1.2-nm-thick Au film after annealing at 300 °C, i.e., below the eutectic temperature T_E. In contrast with the as-deposited pattern, we observe here the appearance of three-dimensional (3D) spots, which can be attributed to the transmission diffraction effect across Au platelets as observed in Fig. 3(a). The 3D spots are arranged in a pseudohexagonal symmetry and the fact that all these spots are located along the (1×1) streaks confirms that these

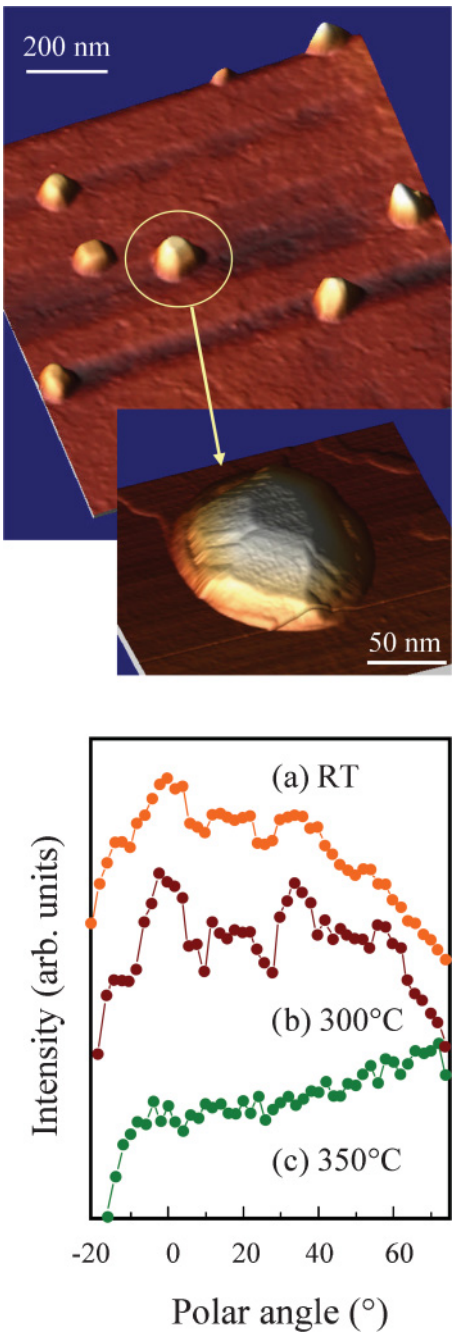

FIG. 5. (Color online) (A) STM image of 0.8-nm Au deposited after 12 h annealing at 350 °C and (B) a detail of a droplet. (C) Au $4f_{7/2}$ XPD profiles versus polar angle θ along the [11-2] direction of the Ge(111) substrate measured at room temperature (RT) (a), on the Au deposit annealed at 300 °C (b), and on the Au deposit annealed at 350 °C (c).

platelets are coherent and epitaxial. We note that (1×1) streaks are still present, indicating that the Au wetting layer between platelets remains flat. When annealing at 350 °C [Fig. 7(b)], 3D spots are still present but interestingly they are distributed along concentric rings, a behavior similar to that observed from electron diffraction of a polycrystalline structure.[52–57] This is in line with STM measurement, for which it is, though, difficult to have a good statistics over all orientation of droplets.

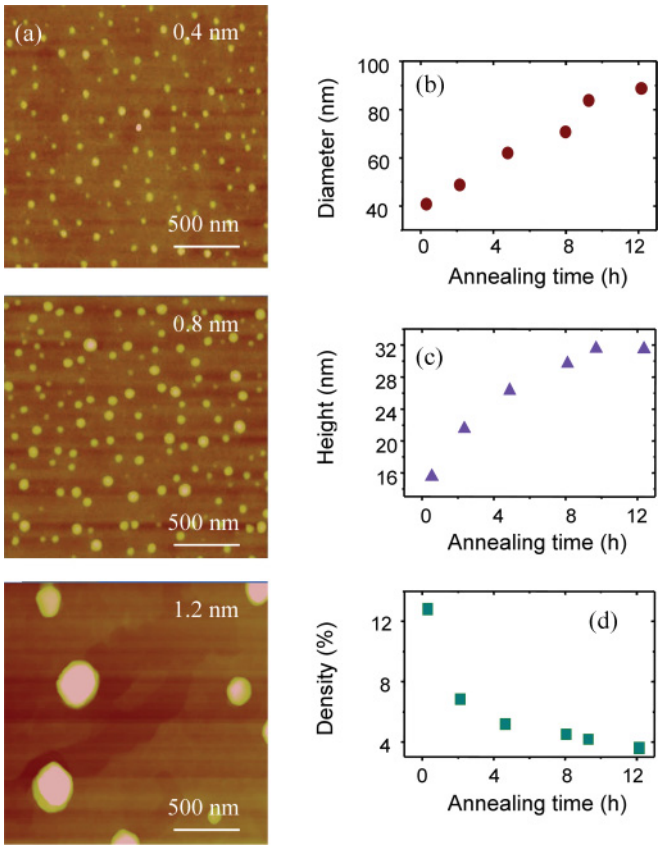

FIG. 6. (Color online) (a) STM images (2 μm × 2 μm) of an Au deposit of 0.4 nm, 0.8 nm, and 1.2 nm annealed at 350 °C for 10 min. Also shown for a 0.8-nm Au deposit annealed at 350 °C. (b) Droplets' diameter versus the annealing time. (c) Droplets' height versus annealing time. (d) Proportion of the surface covered by droplets versus annealing time.

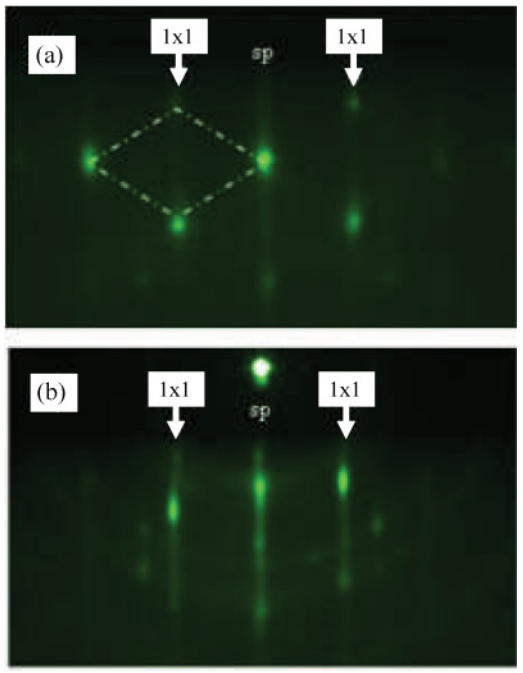

FIG. 7. (Color online) RHEED pattern measured on a 1.2-nm-thick Au layer annealed at 300 °C (a) and 350 °C (b). The primary energy is 30 keV and the angle of incidence is <0.77° from the surface.

This is also in good agreement with the above XPD analyses depicted in the curve c of Fig. 5, which suggests that when Au droplets are formed for annealing at temperatures higher than T_E, they exhibit a random distribution. In other words, upon Ge incorporation the Au-Ge droplets are no longer made up of (111) planes parallel to the (111) plane of Ge substrate but are randomly oriented.

An important question here is is there still Au between the platelets and between the droplets and if so, how much? If it is so, this could also participate in the Au $4f_{7/2}$ modulation versus polar angle. This point has been addressed in the literature a long time ago. Indeed, the formation of the Au-Ge(111) interface has been extensively studied in the 0–1-Au monolayer range, in the two past decades. It has been shown that a $\sqrt{3} \times \sqrt{3}\,R30°$-Au superstructure appears upon annealing a monolayer Au deposit above 300 °C. This superstructure was found to be stable up to the melting point of Ge (958.5 °C). Several atomic models have been proposed for this superstructure. For all models, this superstructure consists of a surface on which Au atoms replace the topmost Ge atoms of the substrate and form trimers. Au atoms replace either the outermost Ge layer or the second Ge layer. This could be in line with the very low solubility of Au in Ge, which is less than 10^{-6} at %.[58–61] However, note that interface formation is generally out of thermodynamical equilibrium, with the formation of new and metastable phases. Anyway, the nominal amount of Au involved in this reconstruction is about one Au monolayer. It was also found that this superstructure induces strong distortion in the deeper Ge layers, with most notably a buckling in the third and fourth Ge layers.[49] For very low coverage, the surface periodicity is more complicated since there was observed a "split" (2 × 2) periodicity along with the $\sqrt{3} \times \sqrt{3}\,R30°$ superstructure.[44] For both Au positions on the Ge(111) surface proposed in the literature, the XPS Au $4f$ wave is not expected to experience forward scattering and its contribution would not be detected at polar angles below 60° in XPS profiles. Some small contribution, as an increase of the mean intensity, would be detected at large polar angles, as it is shown for two-dimensional layers.[62,63] Thus it can be safely assumed that the "bare surface" does not significantly contribute to the Au $4f$ XPD profiles. The Au $4f$ XPD profiles in Figs. 2 and 5 are clearly representative of the Au droplets or platelets, only. The regime of higher Au coverage (more than 1 Au monolayer) has not been so extensively studied, the focus being on the $\sqrt{3} \times \sqrt{3}\,R30°$ itself, due to the universality of its occurrence for the metal/semiconductor interfaces.

Figure 8 shows a SEM image collected at room temperature for a 1.2-nm Au deposit after anneal at 350 °C and 400 °C for 1 h. This deposit is slightly larger than that used for STM, to be easily observed by SEM. STM shows that increasing the deposit from 0.8 to 1.2 nm does not significantly change the surface morphology. Figure 8 shows that each droplet is crystallized, as shown by STM. Also shown is the dispersion in

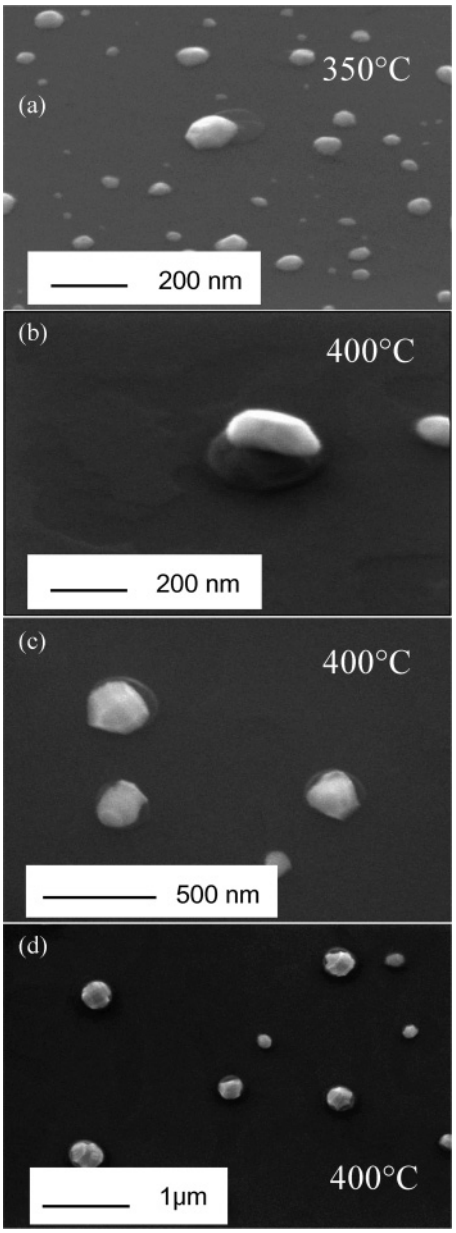

FIG. 8. SEM images collected at room temperature for a 1.2-nm Au deposit after anneal at 350 °C (a) and 400 °C, (b)–(d), for 1 h. The topmost images (a) and (b) are 45° tilted images to enhance the observation of the pedestal. The beam energy is 10 keV.

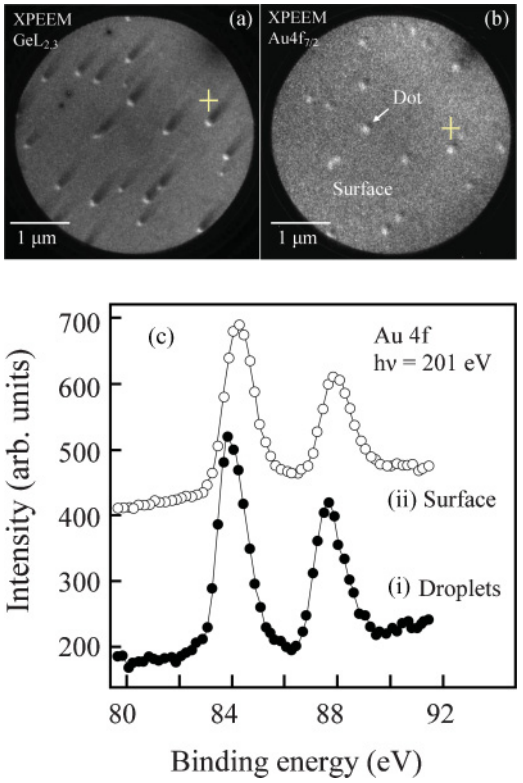

FIG. 9. (a) XPEEM image of the sample surface for 1.2-nm Au deposit annealed at 350 °C for 12 h. This image is acquired in the x-ray-absorption mode, at the Ge $L_{2,3}$ edge, at photon energy of 30 eV. The field of view is 4 μm. (b) XPEEM image acquired in the XPS mode. The sample is illuminated at photon energy of 201 eV and the lateral distribution of the Au 4*f* intensity is taken at a kinetic energy of $E_c = 113$ eV, thus at the Au $4f_{7/2}$ line maximum. (c) Normalized Au 4*f* lines measured on droplets (i) and surface in between (ii).

the crystallized droplets shape, in line with randomly oriented nanocrystals, as suggested by RHEED and STM. Furthermore, one can see that the largest droplets are perched on a pedestal after annealing at 350 °C (for the largest droplets) and 400 °C. This pedestal could be due to precipitated Ge (or Au-Ge alloy), suggesting that quenching of the droplet composition is not completely efficient. The pedestal has a round form, whatever the nanocrystal shape, which is a reminiscence of the liquid droplet form. A similar pedestal has already been observed for Au seeds melt on Si(111). For the Au/Si(111), these pedestals were also attributed to Si precipitation and thus Au and Si phase separation on the basis of selective etching experiments.[64–66] However, the nice experiments reported in Refs. 64 and 65 do not clarify the crucial point of Si-Au alloy formation and composition. A chemical information has thus to be probed by using spectroscopic investigations at a nanometer scale.

Chemical information on Au or Au-Ge nanocrystals is gained by using XPEEM and TEM experiments. These techniques are used in both image and spectroscopy modes. EDX spectroscopy used in TEM with a focalized spot allows a good spatial resolution in cross-section images. Nevertheless, due to the large depth probed by the electrons, it is less suitable for a chemical analysis in the in-plane mode. The analysis of the lateral distribution of Au is more convenient by using a tool such as nanospectromicroscopy XPEEM. This analysis was made by using XPEEM spectral imaging.

Figure 9(a) shows a PEEM image of the sample surface for 1.2-nm Au deposit annealed at 350 °C for 12 h. These experimental conditions are chosen to have droplets large enough to be analyzed since the spatial resolution is about 40 nm in the XPEEM imaging. This image was acquired in the x-ray-absorption mode, at the Ge 3*d* edge. The field of view of this image is 4 μm. Due to the presence of Ge overall sample surface and due to the large depth probed at this photon energy, all parts of the sample appear with the same gray

scale. Nevertheless, thanks to the high photon beam angle, the Au islands are visualized, without significant chemical contrast. The photon beam comes from the bottom left, with an illumination angle of 16° with respect to the surface sample. This image shows Au dots with a diameter in the 150–200-nm range. The topographic contrast is also enhanced by a strong emission of secondary electrons on the bottom-left side of the islands.

The presence of Au atoms between the islands is confirmed by XPEEM, acquired in the XPS mode, and shown in Fig. 9(b). The yellow cross is the reference for both images. Owing to the small Au amount expected between the droplets (1 Au monolayer) and thus in order to maximize surface sensitivity, the photon energy was set to 201 eV, corresponding to a kinetic energy of 113 eV of the Au 4*f* electrons, which is close to the minimum of the inelastic mean free path for this material. This image shows Au dots with a diameter in the 150–200-nm range. The droplets are also visualized thanks to the large illumination angle and to a slight difference in the Au 4*f* intensity between surface and dots. Figure 9(c) shows the Au 4*f* line measured on both droplets and surface in between. These spectra show normalized Au $4f_{7/2}$ intensity versus binding energy E_B. Also scanned during this experiment is the Fermi-level position, in order to have an accurate value of E_B (not shown). The Au 4*f* binding energy E_B measured on droplets is almost the same as for bulk Au at $E_B = 84.0 \pm 0.2$ eV.[48,67–70] This suggests that the droplet surface is almost pure Au. The Au 4*f* lines on droplets and on the bare surface are shifted each other by about 0.45 eV. This chemical shift is consistent with that observed for Au 4*f* measured on the Ge(111)-Au $\sqrt{3} \times \sqrt{3}\,R30°$ surface and on bulk gold.[48] The droplets, with a mean diameter of 150 nm, are large enough to neglect any final-state effect on the Au 4*f* binding energy.[67–70] Note that a straightforward determination of the Au to Ge composition cannot be safely extracted from XPEEM data and it would be only a picture of the droplets for a given growth condition. Indeed, the composition strongly depends not only on the annealing temperature but also on the rate at which the temperature goes down when the sample returns at room temperature. It will be shown below that a strong composition gradient occurs along the surface normal since Ge precipitation is a diffusion limited process. Cross-section TEM images give us more information about the droplet lateral size, the alloyed zone at the Au/Ge(111) interface, and the alloy extension in the droplet and beneath.

Figure 10 show a large scale TEM image with several droplets for an Au deposit of 1.2 nm subsequently annealed at 400 °C. This image clearly shows that all droplets are perched on a pedestal. It is shown that the pedestal lateral extend depends on the droplet: for the droplet on the left, the pedestal extend is quite twice the droplet size while for the droplet on the right, the pedestal extend is quite limited to the droplet lateral size.

Now let us return to the chemical analysis to the interface. Figure 11 shows TEM images along with EDX characterization for a 1.2-nm Au deposit annealed at 350 °C (a: wetting layer), (b: droplet) and 400 °C (c: droplet). Not that for these experiments, the sample temperature was decreased down to room temperature at a rate higher than 10 °C/min. These images show Au-Ge droplets of about 50–100 nm lateral

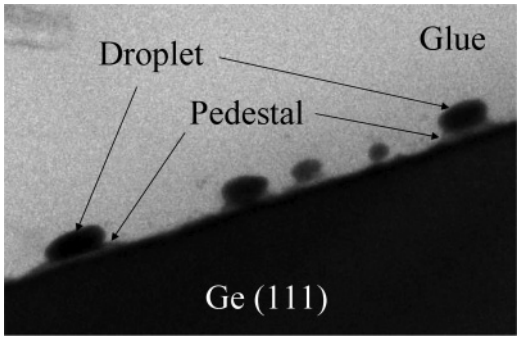

FIG. 10. Cross-section TEM images for a 1.2-nm Au deposit annealed at 400 °C.

size, thus in the range used for XPEEM. It is shown that the dots' height, with respect to the surface plane, is larger after annealing at 400 °C than at $T_E = 350$ °C. Most interestingly, the dots annealed at low temperature (T_E) rest on a 1-nm-thick wetting layer with a quite uniform thickness. In contrast, the dots annealed at higher temperature penetrate more deeply in the Ge(111) substrate. The wetting layer is still observed, with almost the same thickness, but the droplets extend well below the Ge(111)-wetting layer interface. At a first sight, this shows a strong pinning of the droplets when the annealing temperature is increased above T_E. Such self-pinning effect has also been suggested for the Au-Si(111) system by Ferralis *et al.*[65] The present measurements give a direct proof of this effect. Chemical information is given by EDX measurements performed on both droplets' type and also on the wetting layer. Figure 11 shows the GeL, GeK, and AuM lines' intensity across the white line at selected points, for the bare surface (wetting layer), the droplet annealed at 350 °C, and the droplet annealed at 400 °C, respectively. As to the wetting layer, a very small Au signal is detected, in agreement with the formation of a diluted GeAu alloy. All models of the $\sqrt{3} \times \sqrt{3}\,R30°$ reconstruction include only one Au atomic layer on top of the Ge(111). Furthermore, the strong interaction of that single Au layer with the substrate induces strong distortion of the Ge network underneath, as shown by Over *et al.* by using dynamic LEED measurements.[49] These authors proposed Ge displacements up to the sixth atomic plane in the substrate. This could be at the origin of the contrast observed by TEM. Nevertheless, the extent of the wetting layer observed by TEM seems too large compared to that proposed in Refs. 47–49. A part of the wetting layer observed by TEM could also be associated with in-plane Ge precipitation. This point deserves further investigation, in connection with the formation of the pedestal also.

As to the droplets, Fig. 11 shows Ge and Au signals on droplets annealed at 350 °C, i.e., close to the eutectic temperature T_E, and at 400 °C. Upon annealing at 350 °C, the Au signal is clearly sizeable for two points only, namely points 3 and 4, thus in the droplet and above the wetting layer. In line with that, the Ge signal is at its maximum for points 1 and 2, in the substrate or wetting layer, and decreases strongly in the droplet. This graph shows that the Au content is almost the same at the droplet base and on the top of it and indicates that the Au to Ge composition is quite uniform in the droplet upon annealing at T_E. In contrast, the Au

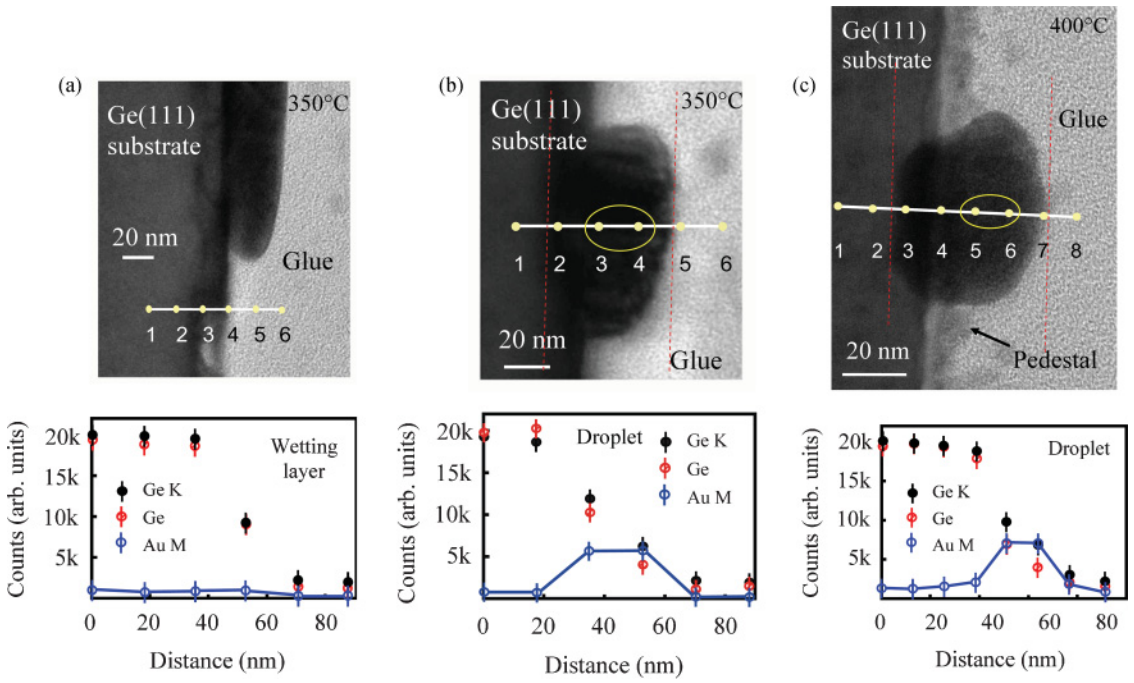

FIG. 11. (Color online) Cross-section TEM images for a 1.2-nm Au deposit annealed at 350 °C, (a)–(e) and 400 °C, (c) and (f). This figure also shows the Ge *L*, Ge *K*, and Au *Mα* lines intensity across the yellow line of the cross-section images at selected points.

signal intensity depends on position in the droplet annealed at 400 °C. Indeed, a large Au signal is only measured at points 5 and 6 although the droplet extends from point 3 to point 7. For points 5 and 6, a smaller Au signal is measured, larger than that at points 1 and 2, which are located in the substrate. These measurements clearly show that the vertical growth of the droplet is associated with a severe Au redistribution in it. The EDX profiles suggest that the Ge to Au composition is quite the same at the points at which the Au*M* line is at maximum. At annealing temperature higher than T_E, a larger amount of Ge is incorporated in the droplet, which increases in height. From the bulk phase diagram, the alloy composition is expected to change from $Au_{78}Ge_{28}$ to $Au_{74}Ge_{32}$ when the annealing temperature is increased from 350 °C to 400 °C. Ge incorporated during the annealing process is now precipitated along the surface plane. It gives a contribution visible by SEM as a pedestal. This pedestal also contributes to the measured Au droplet height, as show in Fig. 11. Nevertheless, the composition variation from $Au_{78}Ge_{28}$ to $Au_{74}Ge_{32}$ upon increasing the temperature at 400 °C seems too low to have such effect on the droplet shape and Ge distribution in it. This would only explain a height increase of about 4%, i.e., far from that observed in Fig. 11. This seems also suggested by the SEM tilted image shown in Fig. 8. The driving force for the longitudinal droplet growth is then the Ge incorporation process during temperature increase, thus climbing the phase diagram liquidus/solidus (L-S) line, and Ge precipitation during temperature decrease, thus going down the L-S line. Nevertheless, this process alone cannot explain the large change in volume occupied by this extra Ge. Surface energy driven agglomeration has to be considered and the bulk phase diagram is modified for the present Au-Ge droplets. Experimental evidence has also been reported at the Au-Ge–Ge interface on top of a Ge nanowire.[23,27,71,72] It was found that for droplets with diameter lower that 100 nm, an important change in the Ge at % is observed. This amounts to about 47% at 450 °C instead of 32% for bulk material, for a Ge nanowire diameter of 32 nm. Nevertheless, this effect is much weaker for droplets on top of Ge nanowires with diameter of 200 nm or more. Some important difference has, though, to be considered: in the present work, the droplet is in contact with a two-dimensional surface (reservoir) instead of a wire.[27] The present experiments suggest that this phenomenon could be enhanced on a two-dimensional surface. This opens the way to large surface modification, via significant material transport across the surface by using the peculiar properties of the binary or ternary alloys with a deep eutectic point in the bulk phase diagram.

IV. CONCLUSION

We have investigated the formation of Au-Ge seeds formed by Au layer dewetting on Ge(111) clean surface. We have shown that they are crystallized after melt and cooling down to room temperature. The Au platelets are in epitaxy on Ge(111) but epitaxy is lost after melt. As expected from bulk phase diagram, Au seeds incorporate Ge, which precipitates to form a pedestal upon cooling down the sample at room temperature. The interesting feature here is that the Ge precipitated amount is larger (at least twice) than expected from the bulk phase diagram opening the way to large surface modification, via significant material transport across the surface.

ACKNOWLEDGMENT

This work was supported by the French National Research Agency Contract No. ANR Blanc 2008 Mag2Wires.

*carmelo.pirri@uha.fr

[1] R. S. Wagner and W. C. Ellis, Appl. Phys. Lett. **4**, 89 (1964).
[2] L. C. Chuang, M. Moewe, C. Chase, N. P. Kobayashi, C. Chang-Hasnain, and S. Crankshaw, Appl. Phys. Lett. **90**, 043115 (2007).
[3] S. M. Prokes and K. L. Wang, Mater. Res. Sci. Bull. **24**, 13 (1999).
[4] X. Duan, Y. Huang, Y. Cui, J. Wang, and C. M. Lieber, Nature (London) **409**, 66 (2001).
[5] Y. Cui and C. M. Lieber, Science **291**, 851 (2001).
[6] A. M. Morales and C. M. Lieber, Science **279**, 208 (1998).
[7] N. Wang, Y. H. Tang, Y. F. Zhang, C. S. Lee, and S. T. Lee, Phys. Rev. B **58**, R16024 (1998).
[8] N. R. B. Coleman, M. A. Morris, T. R. Spalding, and J. D. J. Holmes, Am. Chem. Soc. **123**, 187 (2001).
[9] Y. Wu and P. Yang, Chem. Mater. **12**, 605 (2000).
[10] Y. F. Zhang, Y. H. Tang, N. Wang, C. S. Lee, I. Bello, S. T. Lee, Phys. Rev. B **61**, 4518 (2000).
[11] H. Omi and T. Ogino, Appl. Phys. Lett. **71**, 2163 (1997).
[12] N. R. B. Coleman, K. M. Ryan, T. R. Spalding, J. D. J. Holmes, and M. A. Morris, Chem. Phys. Lett. **343**, 1 (2001).
[13] J. R. Heath and F. K. LeGoues, Chem. Phys. Lett. **208**, 263 (1993).
[14] S. Kodambaka, J. Tersoff, M. C. Reuter, and F. M. Ross, Science **316**, 729 (2007).
[15] G. A. Bootsma and H. J. Gassen, J. Cryst. Growth **10**, 223 (1971).
[16] H. Adhikari, A. F. Marshall, C. E. D. Chidsey, and P. C. McIntyre, Nano Lett. **6**, 318 (2006).
[17] Yajaira Sierra-Sastre, Shadi A. Dayeh, S. T. Picraux, and Carl A. Batt, ACS Nano **4**, 1209 (2010); J. Am. Chem. Soc. **130**, 10489 (2008).
[18] A. F. Marshall, I. A. Goldthorpe, H. Adhikari, M. Koto, Y.-C. Wang, L. Fu, E. Olsson, and P. C. McIntyre, Nano Lett. **10**, 3302 (2010).
[19] A. D. Gamalski, J. Tersoff, R. Sharma, C. Ducati, and S. Hofmann, Nano Lett. **10**, 2972 (2010).
[20] H. Adhikari, A. F. Marshall, I. A. Goldthorpe, C. E. D. Chidsey, and P. C. McIntyre, ACS Nano **1**, 415 (2007).
[21] S. A. Dayeh and S. T. Picraux, Nano Lett. **10**, 4032 (2010).
[22] Y. Wu and P. Yang, J. Am. Chem. Soc. **123**, 3165 (2001).
[23] E. Sutter and P. Sutter, Nanoletters **8**, 411 (2008).
[24] X. Li, G. Meng, Q. Xu, M. Kong, X. Zhu, Z. Chu, and A.-P. Li, Nano Lett. **11**, 1704 (2011).
[25] K. Kang, D. A. Kim, H. S. Lee, C. J. Kim, J. E. Yang, and M. H. Jo, Adv. Mater. **20**, 4684 (2008).
[26] M. Ge, J. F. Liu, H. Wu, C. Yao, Y. Zeng, Z. D. Fu, S. L. Zhang, and J. Z. Jiang, J. Phys. Chem. C **111**, 11157 (2007).
[27] E. Sutter and P. Sutter, ACS Nano **4**, 4943 (2010).
[28] K. W. Schwarz and J. Tersoff, Nano Lett. **11**, 316 (2011).
[29] V. G. Dubrovskii, G. E. Cirlin, N. V. Sibirev, F. Jabeen, J. C. Harmand, and P. Werner, Nano Lett. **11**, 1247 (2011).
[30] E. Sutter and P. Sutter, Adv. Mater. **18**, 2583 (2006).
[31] T. Hanrath and B. A. Korgel, J. Am. Chem. Soc. **124**, 1424 (2002).
[32] P. C. McIntyre, H. Adhikari, I. A. Goldthorpe, S. Hu, P. W. Leu, A. F. Marshall, and C. E. Chidsey, Semicond. Sci. Technol. **25**, 024016 (2010).
[33] H. Adhikaria, P. C. McIntyre, A. F. Marshall, and C. E. D. Chidsey, J. Appl. Phys. **102**, 094311 (2007).
[34] W. H. Chen, R. Lardé, E. Cadel, T. Xu, B. Grandidier, J. P. Nys, D. Stiévenard, and P. Pareige, J. Appl. Phys. **107**, 084902 (2010).
[35] Di Gao, R. He, C. Carraro, R. T. Howe, P. Yang, and R. Maboudian, J. Am. Chem. Soc. **127**, 4574 (2005).
[36] A. Kramer, T. Boeck, P. Schramm, and R. Fornari, Physica E **40**, 2462 (2008).
[37] Y. Homma, P. Finnie, T. Ogino, H. Noda, and T. Urisu, J. Appl. Phys. **86**, 3083 (1999).
[38] Y. Sierra-Sastre, S. Choi, S. T. Picraux, and C. A. Batt, J. Am. Chem. Soc. **130**, 10488 (2008).
[39] S. N. Mohammad, J. Chem. Phys. **131**, 224702 (2009).
[40] B. Fuhrmann, H. S. Leipner, H.-R. Ho1che, L. Schubert, P. Werner, and U. Gösele, Nano Lett. **5**, 2524 (2005).
[41] T. Xu, J. P. Nys, A. Addad, O. I. Lebedev, A. Urbieta, B. Salhi, M. Berthe, B. Grandidier, and D. Stiévenard, Phys. Rev. B **81**, 115403 (2010).
[42] Y. Margoninski and L. G. Feinstein, Surf. Sci. **23**, 458 (1970).
[43] G. Le Lay, M. Manneville, and J. J. Métois, Surf. Sci. Lett. **123**, A445 (1982).
[44] G. Le Lay, M. Manneville, and J. J. Métois, Surf. Sci. **123** 117 (1982).
[45] P. Perfetti, A. D. Katnani, R. R. Daniels, Te-Xiu Zhao, and G. Margaritondo, Solid State Commun. **41**, 213 (1982).
[46] L. Seehofer and R. L. Johnson, Surf. Sci. **318**, 21 (1994).
[47] P. B. Howes, C. Norris, M. S. Finney, E. Vlieg, and R. G. van Silfhout, Phys. Rev. B **48**, 1632 (1993).
[48] M. Göthelid, M. Hammar, M. Björkqvist, U. O. Karlsson, S. A. Flodström, C. Wigren, and G. LeLay, Phys. Rev. B **50**, 4470 (1994).
[49] H. Over, C. P. Wang, and F. Jona, Phys. Rev. B **51**, 4231 (1995).
[50] A. Locatelli, A. Bianco, D. Cocco, S. Cherifi, S. Heun, M. Marsi, and E. Bauer, J. Phys. IV **104**, 99 (2003).
[51] A. Locatelli, L. Aballe, T. O. Mentes, M. Kiskinova, and E. Bauer, Surf. Interface Anal. **38**, 1554 (2006).
[52] M. Derivaz, P. Noé, R. Dianoux, A. Barski, T. Schülli, and T. H. Metzger, Appl. Phys. Lett. **81**, 3843 (2002).
[53] R. T. Brewer, H. A. Atwater, J. R. Groves, and P. N. Arendt, J. Appl. Phys. **93**, 205 (2003).
[54] J. T. Drotar, T. M. Lu, and G. C. Wang, J. Appl. Phys **96**, 7071 (2004).
[55] T. Feng, H. Yu, M. Dicken, J. R. Heath, and H. A. Atwater, Appl. Phys. Lett. **86**, 033103 (2005).
[56] Á. Nemcsics, Ch. Heyn, A. Stemmann, A. Schramm, H. Welsch, and W. Hansen, Mater. Sci. Eng. B **165**, 118 (2009).
[57] R. Krishnan, Y. Liu, C. Gaire, L. Chen, G.-C. Wang, and T. M. Lu, Nanotechnology **21**, 325704 (2010).
[58] R. M. Waghorne, V. G. Rivlin, and G. I. Williams, J. Phys. F **6**, 147 (1976).
[59] R. P. Elliott and F. A. Shunk, J. Phase Equilib. **1**, 51 (1980).
[60] *Binary Alloy Phase Diagrams*, 2nd ed., Vol. 1 (ASM International: Materials Park, OH, 1990).
[61] D. Hourlier and P. Perrot, Mater. Sci. Forum **653**, 77 (2010).
[62] P. Wetzel, C. Pirri, P. Paki, D. Bolmont, and G. Gewinner, Phys. Rev. B **47**, 3677 (1993).
[63] P. Wetzel, C. Pirri, and G. Gewinner, Europhys. Lett. **38**, 359 (1997).
[64] B. Ressel, K. C. Prince, S. Heun, and Y. Homma, J. Appl. Phys. **93**, 3886 (2003).
[65] N. Ferralis, R. Maboudian, and C. Carraro, J. Am. Chem. Soc. **130**, 2683 (2008).
[66] N. Ferralis, F. El Gabaly, A. K. Schmid, R. Maboudian, and C. Carraro, Phys. Rev. Lett. **103**, 256102 (2009).

[67] S. Shukla and S. Seal, Nano Struct. Mater. **11**, 1181 (1999).
[68] A. Tanaka, Y. Takeda, T. Nagasawa, and K. Takahashi, Solid State Commun. **126**, 191 (2003).
[69] A. Tanaka, Y. Takeda, M. Imamura, and S. Sato, Phys. Rev. B **68**, 195415 (2003).
[70] T. Ohgi and D. Fujita, Surf. Sci. **532–535**, 294 (2003).
[71] P. W. Sutter and E. A. Sutter, Nat. Mater. **6**, 363 (2007).
[72] J. Guzman, C. N. Boswell-Koller, J. W. Beeman, K. C. Bustillo, T. Conry, O. D. Dubón, W. L. Hansen, A. X. Levander, C. Y. Liao, R. R. Lieten, C. A. Sawyer, M. P. Sherburne, S. J. Shin, P. R. Stone, M. Watanabe, K. M. Yu, J. W. Ager III, D. C. Chrzan, and E. E. Haller, Appl. Phys. Lett. **98**, 193101 (2011).